



ORIGINAL ARTICLE

Suppression of adipogenesis by Au nanostructures-conjugated *Sargassum* seaweed extracts in 3 T3-L1 adipocytes



Sun Young Park ^{a,*}, Beomjin Kim ^b, Yeong Jin Kim ^c, Hyung-Hoi Kim ^{c,d},
Jin-Woo Oh ^{a,b,*}, Geuntae Park ^{a,b,*}

^a Bio-IT Fusion Technology Research Institute, Pusan National University, Busan 46241, Republic of Korea

^b Department of Nano Fusion Technology, Graduate School, Pusan National University, Busan 46241, Republic of Korea

^c Biomedical Research Institute, Pusan National University Hospital, Busan 49241, Republic of Korea

^d Department of Laboratory Medicine, Pusan National University Hospital, Busan 49241, Republic of Korea

Received 19 May 2022; accepted 30 June 2022

Available online 5 July 2022

KEYWORDS

Sargassum siliquastrum;
Sargassum horneri;
AuNPs;
Adipogenesis

Abstract Recently, with the development of metal nanostructure synthesis technology, Au nanostructures (AuNPs) are synthesized using seaweed extract without using an organic solvent and applied to the pharmaceutical field. In this regard, in this study, AuNPs biosynthesis was mediated through extracts of two brown algae (*Sargassum siliquastrum* [SS] and *Sargassum horneri* [SH]) without the use of stabilizers or surfactants. In addition, we investigated the effects of SS-AuNPs (SS-functionalized AuNPs) and SH-AuNPs (SH-functionalized AuNPs) on adipogenesis in adipocytes and their underlying molecular mechanisms. A rapid and simplified synthesis of SS-AuNP and SH-AuP was achieved using aqueous extracts of SS and SH. The morphology, structure and composition of SS-AuNPs and SH-AuNPs were characterized by DLS, FTIR, UV-Vis spectroscopy, HR-TEM and EDS analysis. The stable monodisperse SS-AuNPs and SH-AuPs were synthesized with mean sizes of 17.47 ± 0.13 nm and 21.0 ± 2.74 and zeta potentials of -31.9 ± 0.75 and -34.57 ± 4.43 , the biosynthetic AuNPs with the face-centered structure of SS-AuNPs and SH-AuPs had crystalline characteristics, and many functional groups that play an important role in the biological reduction present in the SS and SH extracts were adsorbed on the surfaces of the SS-AuNPs and SH-AuPs. This study was conducted to investigate the effect of SS-AuNPs and

* Corresponding authors at: Department of Nanofusion Technology, Graduate School, Pusan National University, Busan 46241, Republic of Korea (G. Park and J.-W. Oh), Bio-IT Fusion Technology Research Institute, Pusan National University, 2, Busandaehak-ro 63beon-gil, Geumjeong-gu, Busan 46241, Republic of Korea (S. Y. Park).

E-mail addresses: sundeng99@pusan.ac.kr (S. Young Park), ojw@pusan.ac.kr (J.-W. Oh), gtpark@pusan.ac.kr (G. Park).

Peer review under responsibility of King Saud University.



SH-AuPs on adipogenesis in adipocytes. SS-AuNPs and SH-AuPs reduced morphological changes and increased lipid accumulation by approximately 80% compared with that in mature adipocytes (MDI-induced). This result was accompanied by a reduction in the triglyceride content. SS-AuNPs and SH-AuPs suppressed lipid accumulation by downregulating C/EBP α , PPAR γ , SREBP 1, FAS, and aP2 mRNA and protein expression. Furthermore, SS-AuNPs and SH-AuPs induced the mRNA and protein expression of UCPI1, PRDM16, and PGC1 α to increase mitochondrial biogenesis in mature adipocytes and effectively induced brown adipogenesis. SS-AuNPs and SH-AuPs have potent anti-adipogenic effects and can be used as potential therapeutic agents for obesity.

© 2022 The Author(s). Published by Elsevier B.V. on behalf of King Saud University. This is an open access article under the CC BY-NC-ND license (<http://creativecommons.org/licenses/by-nc-nd/4.0/>).

1. Introduction

Metal nanostructures are used as biosensors and gene-targeted drug delivery systems in the medical field because of their easy surface modification, uniform particle size distribution, and excellent stability (Machado et al., 2021; Andleeb et al., 2021). Metal nanostructures vibrate free electron clouds through mutual interference with electromagnetic waves of external light to form surface plasmon resonance and exhibit biocompatibility properties. Specifically, Au nanostructures (AuNPs) can be easily integrated with biological molecules because of their low biotoxicity, and their ability to adsorb various organic ligands to the surface (Holišová et al., 2021; Boomi et al., 2020; Nayem et al., 2020). AuNPs can be synthesized using physical and chemical methods. For physical synthesis, expensive equipment is required, and controlling the size of nanostructures is difficult. In the case of chemical synthesis, the process is simple but expensive and has the side effect of reducing agents. Accordingly, active research is being conducted to devise a method for AuNPs biosynthesis without the use of organic solvents (Park, S. Y. et al., 2020; Jun et al., 2020). Natural resource-derived extracts have been used as reducing agents and stabilizers as they impart positive biological activity when applied to humans. As a result, there is increasing interest in various scientific fields such as medicine and the environment (Lee, K. X. et al., 2020; Khan et al., 2019).

Obesity is caused by an imbalance in food intake and energy use and can lead to serious diseases such as inflammation, type 2 diabetes, and arteriosclerosis. The aforementioned three diseases are collectively referred to as “metabolic syndrome” (Molina-Ayala et al., 2022; Yang et al., 2021; Vasileva et al., 2021). Because this geriatric disease occurs in the most active individuals in society, the economic loss is great, and the cost of prevention and treatment is highest in the pharmaceutical and health industries. Adipocytes and adipose tissues play important roles in obesity (Sprenger et al., 2022; Jee et al., 2021; Borah et al., 2021). They are simultaneously metabolic organs that integrate multiple physiological pathways and endocrine organs that secrete hormones and cytokines essential for systemic insulin sensitivity and energy production. Adipocytes store fat in the form of triglycerides (TGs). When available glycogen sources in the body are depleted by exercise or fasting, they break down stored TGs to promote energy generation and play a pivotal role in maintaining blood sugar homeostasis. However, the normal differentiation process of preadipocytes into adipocytes occurs abnormally through hyperdifferentiation. Obesity at the cellular level is caused by an increase in the number and volume of adipocytes through the promotion of their proliferation and differentiation. Therefore, controlling adipogenesis the process of differentiation from preadipocytes to mature adipocytes is an important step in obesity treatment (Moon et al., 2013; Ho et al., 2012; Abbas et al., 2022).

The aberrant differentiation process of adipocytes involves the interaction of several markers, including nutrients and hormones, and is precisely regulated by positive and negative interactions of molecules involved in insulin-related signaling pathways and various transcription factors. These interactions also lead to morphological

changes in adipocytes and changes in gene expression levels at the transcriptional stage. Transcription factors, such as C/EBP, PPAR, and ADD1/SREBP 1C, play essential roles in regulating adipocyte differentiation. These transcription factors regulate the expression of adipocyte-specific genes, such as FAS and aP2, and induce the activation of fat metabolism and adipocyte differentiation (Yan et al., 2022; Pinto et al., 2021; Ree et al., 2021). Therefore, research is necessary to identify candidate molecules that inhibit adipocyte differentiation and reduce adipocyte production and fat accumulation. The in vitro cell line model 3 T3-L1 pre-adipocytes is mainly used to study adipocyte proliferation and differentiation. When treating 3 T3-L1 pre-adipocytes with hormone stimulants such as 3-isobutyl-1-methylxanthine, dexamethasone, or insulin (MDI), they undergo a mitotic clonal expansion phase in which cell division is resumed. At the same time, the expression of specific genes involved in the development of adipocytes, such as C/EBP α , PPAR γ , SREBP 1, FAS, and aP2, appears, and finally, the process of adipocyte differentiation progresses (Park, M. et al., 2022; Lim et al., 2021; Du et al., 2022).

Recently, research is being conducted to develop various functional materials using seaweed extract to utilize the biological benefits of seaweed. *Sargassum siliquastrum* (SS) and *Sargassum horneri* (SH) are brown algae that grow beneath reef waters. Their composition includes dextrose, crude fiber, fat, crude protein, pure protein, ash, iron, calcium, amino acids, phosphorus, and other minerals. SS and SH are mainly distributed in Korea, Japan, and China, where young individuals are edible (Fernando et al., 2020; Herath et al., 2021; Dias et al., 2021). SS and SH have antioxidant, antibacterial, anticancer, anti-inflammatory, blood-pressure lowering, lipid-lowering, and radioisotope-excretion properties (Kim et al., 2021; Lee, J. I. et al., 2013; Dias et al., 2021). Therefore, in this study, we examined the effect of SS-AuNPs (SS-functionalized AuNPs) and SH-AuNPs (SH-functionalized AuNPs) on MDI-induced mature adipocytes and the potential mechanism for mediating its effects. According to our review of the literature, this study is the first comparative examination of SS-AuNPs and SH-AuNPs for selective biosynthesis using brown algae.

2. Material and methods

2.1. Preparation of SS and SH extracts

SS and SH were provided by Jeju Technopark Biodiversity Research Institute (voucher specimens No. JBRI-16030(SS), No. JBRI-16072(SH)). Specimens of SS and SH are deposited at the Herbarium of the Jeju Institute of Biological Diversity in Jeju, and SS and SH were identified by Dr. Wookjae Lee (Jeju Technopark, Jeju). SS and SH specimens were harvested from the shores of Jeju Island in Jeju Province, Korea. They were cleaned and dried in a cool place. SS and SH specimens were dehydrated and uniformed into a fine powder (HMF-3100S, Hanil Electric, Seoul, Korea) by using an electric mixer. We used 40–50 mesh standard test sieves to separate and obtain

the smallest possible sizes of the SS and SH powders. Next, we prepared the SS and SH extract solutions: 10 g each of well-ground SS and SH was mixed in 300 mL of % ethanol and extracted at room temperature for 12 h, they were then centrifuged at $6000 \times g$ for 10 min to obtain a supernatant. The SS and SH extracts were filtered and concentrated using a rotary vacuum evaporator (Buchi Rotavapor R-144, Buchi Labortechnik, Flawil, Switzerland) and freeze-dried. The SS and SH powders were preserved at $-80\text{ }^{\circ}\text{C}$ until needed. The SS and SH powders were dissolved in an aqueous solution at a concentration of 4 mg/mL by using SS and SH-AuNPs media. The solution was then filtered and sterilized using a $0.2\text{ }\mu\text{m}$ syringe filter.

2.2. Synthesis of AuNPs factionalized with SS and SH extract

AuNPs was synthesized by optimizing the concentration, temperature, and reaction time of the SS and SH extracts and metal precursors. First, an aqueous solution of 1 M $\text{HAuCl}_4 \cdot 3\text{H}_2\text{O}$ was added to the filtered SH extract (4 mg/mL) and incubated in water at $80\text{ }^{\circ}\text{C}$ for 15 min. Next, the tubes containing the colloid were placed on ice for 5 min. The color of the suspension changed to dark purple, indicating the successful synthesis of SS and SH-AuNPs.

2.3. Physicochemical characterization of SS and SH-AuNPs

The formation of SS-AuNPs and SH-AuNPs was analyzed using an Ultrospec 6300 pro-UV-Vis spectrophotometer (Amersham Biosciences, Buckinghamshire, UK) within a wavelength range of 300–800 nm. The size, zeta potential, and polydispersity index (PDI) values of the SS-AuNPs and

SH-AuNPs were determined using a Zetasizer Nano-ZS90 (Malvern Panalytical, Malvern, UK). The morphology and particle size distributions of SS-AuNPs and SH-AuNPs were obtained using high-resolution transmission electron microscopy (HR-TEM; ALOS F200X (Thermo Scientific, Oregon, USA) operated at a potential of 200 kV. For confirming that SS-AuNPs and SH-AuNPs were synthesized from SS and SH extracts, Fourier-transform infrared (FTIR) spectra were analyzed using a Spectrum GX spectrometer (Perkin Elmer Inc., Boston, MA, USA) equipped with potassium bromide pellets.

2.4. Pre- and mature adipocyte culture and treatment

Mouse 3 T3-L1 pre-adipocytes (CL-173, Lot:70047755) were obtained from the American Type Culture Collection (Manassas, VA, USA) and cultured in Dulbecco's modified eagle medium/ nutrient mixture F-12 containing 10% fetal bovine serum and 1% penicillin–streptomycin. To obtain mature adipocytes, we incubated pre-adipocytes as aforementioned until they reached confluence. The medium was replaced 2 d later and differentiation was induced using the 3 T3-L1 Differentiation Kit (BioVision, Milpitas, CA, United States). The adipocytes were incubated for 3 d in the differentiation medium (MDI differentiation medium: $1\text{ }\mu\text{M}$ dexamethasone, $500\text{ }\mu\text{M}$ IBMX, $1.5\text{ }\mu\text{g/mL}$ insulin, and $1\text{ }\mu\text{M}$ rosiglitazone). Adipocytes cultured for 3 d were cultured for an additional 2 d in Dulbecco's modified eagle medium/ nutrient mixture F-12 containing $1.5\text{ }\mu\text{g/mL}$ insulin. Thereafter, the culture medium of the adipocytes was replaced every 2 d. Next, we evaluated the anti-adipogenic effect by administering SS and SH-AuNPs ($10\text{--}20\text{ }\mu\text{g/mL}$) 2 h before exposure to the MDI differentiation medium for 9 d (Fig. 1).

Adipocyte Differentiation and Treatment

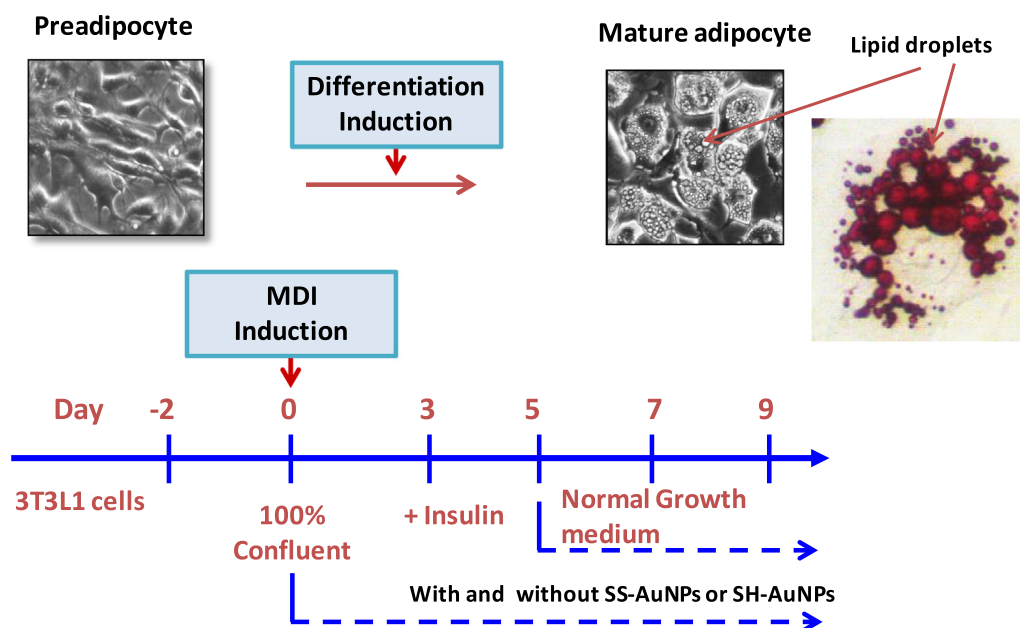


Fig. 1 Experimental design of pre- and mature- adipocyte culture and treatment.

2.5. Cell viability of pre- and mature adipocytes

The Cell Counting Kit 8 (CCK 8) Assay Kit (Sigma-Aldrich–Merck KGaA, Burlington, MA, USA) was used for cell viability assays using pre- or mature adipocytes. Cells were seeded in a 48-well plate at a concentration of 1×10^4 cells and incubated at 37 °C with 5% CO₂. After 2 d of incubation, SS and SH-AuNPs were pretreated with 0, 1, 2.5, 5, 10, 20, and 40 µg/mL for 2 h and then either treated or not treated with MDI differentiation medium. CCK-8 reagent was added to each well at a concentration of 1/100, wrapped in foil, and incubated for 4 h. Cells were quantified by measuring the absorbance at 450 nm using a Wallac Victor plate reader (Perkin Elmer Corp., Norwalk, CT).

2.6. Lipid droplet measurement using Oil Red-O and Nile-red staining

After inducing adipocyte differentiation for 9 d, the cells were stained on day 9 using a lipid (Oil Red-O) staining kit (BioVision, Milpitas, CA, United States) and Nile-red staining kit (Abcam, Cambridge, UK). Briefly, mature adipocytes were washed twice with phosphate-buffered saline, fixed with 10% formalin, and stained with Oil Red-O solution for 1 h at room temperature. After 1 h, the Oil Red-O staining solution was removed, and images of the stained lipid droplets were taken with an optical microscope. For the quantification of lipid droplets, the Oil Red-O staining reagent remaining in the cells was dissolved in isopropanol and separated, and the absorbance was measured at 490 nm. For Nile-Red staining, 4,000 preadipocytes were cultured in 8-well chamber slides (Thermo Fisher Scientific Life Sciences); next, mature adipocytes were induced using the aforementioned method. Mature adipocytes were rinsed with phosphate-buffered saline, fixed with 10% formalin buffer, and stained with Nile-Red solution for 30 min at room temperature. Images of the stained lipid droplets were captured using a confocal microscope (LSM 800, Carl Zeiss, Jena, Germany) and quantified based on a fluorescence unit using a fluorescent dye in a flow cytometer (Fit NxT Flow Cytometer; Thermo Fisher Scientific, Inc.).

2.7. TG analysis

To control intracellular TG levels, we inoculated preadipocytes at 2×10^6 cells per well in six wells, and reagent treatment and differentiation were induced according to the aforementioned method. A triglyceride colorimetric assay kit (Cayman Chemical Company, MI, USA) was used to measure

TG levels. The protein concentration in the cell lysate was determined using the Bio-Rad protein assay kit.

2.8. Reverse-transcription quantitative polymerase chain reaction (RT-qPCR)

Total RNA was extracted from the adipocytes by using the RNeasy Mini Kit (Qiagen GmbH). RNA concentration was determined using a NanoDrop spectrophotometer (Thermo Scientific, USA). Subsequently, cDNA was synthesized using a high-dose cDNA reverse kit (Applied Biosystems, CA, USA). The relative quantification of gene expression was performed using SYBR Green qPCR Master Mix (Applied Biosystems, Bio-Rad Laboratories, Inc.) and Bio-Rad Chromo4™ (Applied Biosystems, CA, USA). Samples were amplified in triplicate in 96-well plates, with 40 cycles at 95 °C for 15 s and 58 °C for 40 s. The primers used are listed in Table 1. Data were analyzed using $2^{-\Delta\Delta CT}$.

2.9. Western blotting

Adipocytes were lysed using a mammalian protein extraction reagent (Thermo Fisher Scientific, USA) containing a protease inhibitor (Sigma-Aldrich, USA). The mixture was placed on ice for 30 min, shaken every few minutes, and then centrifuged at 12,000 rpm under 4 °C for 10 min. The supernatant was collected, and the protein concentration was measured using the Bio-Rad protein assay kit (Bio-Rad Laboratories, Inc.). Mini-PROTEAN Precast Gels (Bio-Rad Laboratories, Inc.) were prepared, and the samples were loaded after protein denaturation. A Hybond polyvinylidene difluoride membrane (Amersham, Amersham, UK) was cut out, and the protein was transferred to the membrane. The membranes were blocked for 1 h and incubated overnight at 4 °C with diluted primary antibodies. The primary antibodies used are listed in Table 2. The membranes were then washed three times and incubated with horseradish peroxidase-conjugated secondary antibody for 1 h at room temperature. After washing, the membranes were made to react with enhanced Pierce ECL Western blotting substrate (Thermo Fisher Scientific, USA). The relative intensities of the bands were determined using ImageQuant TL (version 8.1; Amersham, Amersham, UK).

2.10. Immunofluorescence assay

For the immunofluorescence assay, 4,000 preadipocytes were cultured in 8-well chamber slides (Thermo Fisher Scientific Life Sciences); next, mature adipocytes were induced by the

Table 1 Primer sequences used for the qPCR analysis.

Gene	Forward primer	Reverse primer
<i>C/EBPα</i>	TGGTGATTTGTCCGTTGTCT	GGA AACCTGGCCTGTTGTAAG
<i>PPARγ</i>	GGTGATTTGTCCGTTGTCT	GCTTCAATCGGATGGTTCTTC
<i>SREBP-1</i>	TAGAGCATATCCCCAGGTG	GGTACGGGCCACAAGAAGTA
<i>FAS</i>	GCTGCGAAACTTCAGGAAAT	AGAGACGTGTCACTCCTGGACTT
<i>aP2</i>	GGATTGGTACCATCCGGT	TTCACCTTCTGTCTGTCTGC
<i>UCP1</i>	CCTGCCTCTCTCGAAACAA	GTAGCGGGGTTTGATCCCAT
<i>PRDM16</i>	CAGCACGGTGAAGCCATTC	GCGTGCATCCGCTTGTG
<i>PGC1α</i>	ATGTGCAGCCAAGACTCTGTA	CGCTACACCACTTCAATCCAC
<i>GAPDH</i>	AGTCCGGTGTGAACGGATTTG	TGTAGACCATGTAGTTGAGGTCA

Table 2 Antibody information of western blot assays.

Antibody	Company	Catalogue	Species	Dilution
<i>C/EBPα</i>	Cell Signaling	#8178	Rabbit	1:500
<i>PPARγ</i>	Cell Signaling	#2435	Rabbit	1:500
<i>SREBP-1</i>	Santa Cruz	sc-365513	Mouse	1:1000
<i>FAS</i>	Cell Signaling	#3180	Rabbit	1:500
<i>aP2</i>	Cell Signaling	#2120	Rabbit	1:500
<i>UCP1</i>	Santa Cruz	sc-293418	Mouse	1:1000
<i>PRDM16</i>	Abcam	ab106410	Mouse	1:500
<i>PGC1α</i>	Santa Cruz	sc-518025	Mouse	1:500
<i>β-actin</i>	Santa Cruz	sc-47778	Goat	1:1000

aforementioned method. Adipocytes were treated with 0.1% Triton X-100 serum for 30 min and then fixed with 4% paraformaldehyde for 30 min. Permeabilized adipocytes were then blocked with 1% bovine serum albumin in phosphate-buffered saline with Tween 20 for 1 h and incubated overnight with antibodies against uncoupling protein 1 (UCP1) (Alexa Fluor 488 Conjugate, 1:200, Cell Signaling Technology) at 4 °C. Adipocytes were washed three times with phosphate-buffered saline and then incubated with DAPI mounting medium (Sigma-Aldrich; Merck KGaA) for 30 s at 37 °C in the dark. Adipocytes were visualized using a Zeiss LSM 800 confocal laser scanning microscope (Zeiss, Germany).

2.11. Statistical analysis

Statistical analyses were performed using GraphPad Prism 4.0 (GraphPad Software, San Diego, CA, USA). Comparisons of multiple groups were performed using a one-way analysis of variance and Tukey's post hoc test. Statistical significance was set at p value < 0.05. Data are presented as mean \pm standard deviation (SD).

3. Results

3.1. Physicochemical characterization of SS-AuNPs and SH-AuNPs

The SS and SH extracts served as both reducing-capping and stabilizing agents for the reduction and formation of metal salts during the synthesis of AuNPs. The maximum localized surface plasmon resonance peaks of SS-AuNPs and SH-AuNPs were confirmed to be at 528 nm and 525 nm, respectively, as determined by UV-Vis spectroscopy. Table 3 shows the size, zeta potential, and polydispersity indices of SS-AuNPs and SH-AuNPs measured using the scattering method. The average sizes of SS-AuNPs and SH-AuNPs were 17.47 ± 0.13 nm and 21.0 ± 2.74 (Fig. 2A). To verify the stability of AuNPs, we analyzed the zeta potential values and confirmed that the zeta potentials of SS-AuNPs and SH-AuNPs showed

stable values of -31.9 ± 0.75 and -34.57 ± 4.43 , respectively. For observing the shape, size, and dispersion of the biosynthesized SS-AuNPs and SH-AuNPs, a final analysis was performed using HR-TEM. We assessed the TEM image and confirmed that, in addition to other shapes such as pentagons, hexagons, and octagons, most of the nanostructures were spherical and well dispersed without agglomeration. The diameters of SS-AuNPs and SH-AuNPs shown in the TEM images were approximately 11.39–27.81 nm and 7.85–25.63 nm, respectively (Fig. 2B and C). In the high-angle annular dark-field (HAADF) mode of HR-TEM, the distribution of Au in SS-AuNPs and SH-AuNPs was confirmed through the red particle image (Fig. 2D). The selected area electron diffraction (SAED) mode of the HR-TEM shown in Fig. 2E demonstrates that the synthesized nanostructures have a crystalline structure. The bright rings correspond to the (111), (200), (220), and (311) lattice planes, indicating that SS-AuNPs and SH-AuNPs were face-centered cubic structures. The energy-dispersive X-ray spectroscopy (EDX) spectra of SS-AuNPs and SH-AuNPs are displayed in Fig. 2F. SS-AuNPs and SH-AuNPs show peaks at 0.2–0.5, 2–2.4, and 9.5–9.8 keV. FTIR analysis was performed to determine the function of the SS and SH extracts in reducing the capping and stabilizing agents. Using FTIR spectra, we integrated the analysis of potential biomolecules and functional chains responsible for biosynthesis on SS-AuNPs and SH-AuNPs surfaces with SS and SH extracts. The analysis of the SS and SH extracts and SS-AuNPs and SH-AuNPs demonstrated the following: the peaks at 3412(SS) correspond to 3421(SS- AuNPs), 3411(SH) correspond to 3423(SH- AuNPs), 1397(SS) correspond to 1401(SS- AuNPs), and 1396(SH) correspond to 1398(SH- AuNPs) cm^{-1} , corresponding to the stretching of – OH bonds in polyphenols or alcohols, which are chemicals found in brown algae. The peaks at 1592(SS) and 1587(SH) correspond to 1599(SS- AuNPs) and 1595(SH- AuNPs) cm^{-1} , respectively, corresponding to the NH stretching vibration of the amine group. The peak at 1078(SS) corresponds to 1079(SS- AuNPs) cm^{-1} , which is due to the CO stretching of the alcohol (Fig. 2G and H). This suggests that potential biomolecules and functional chains, including amino acids, primary and tertiary ami-

Table 3 Size and Zeta potential of SH-NPs.

Sample	Zeta potential (mV)	Average size (nm)	Polydispersity index
SS-AuNS	-31.9 ± 0.75	17.47 ± 0.13	0.374
SH-AuNS	-34.57 ± 4.43	21.0 ± 2.74	0.360

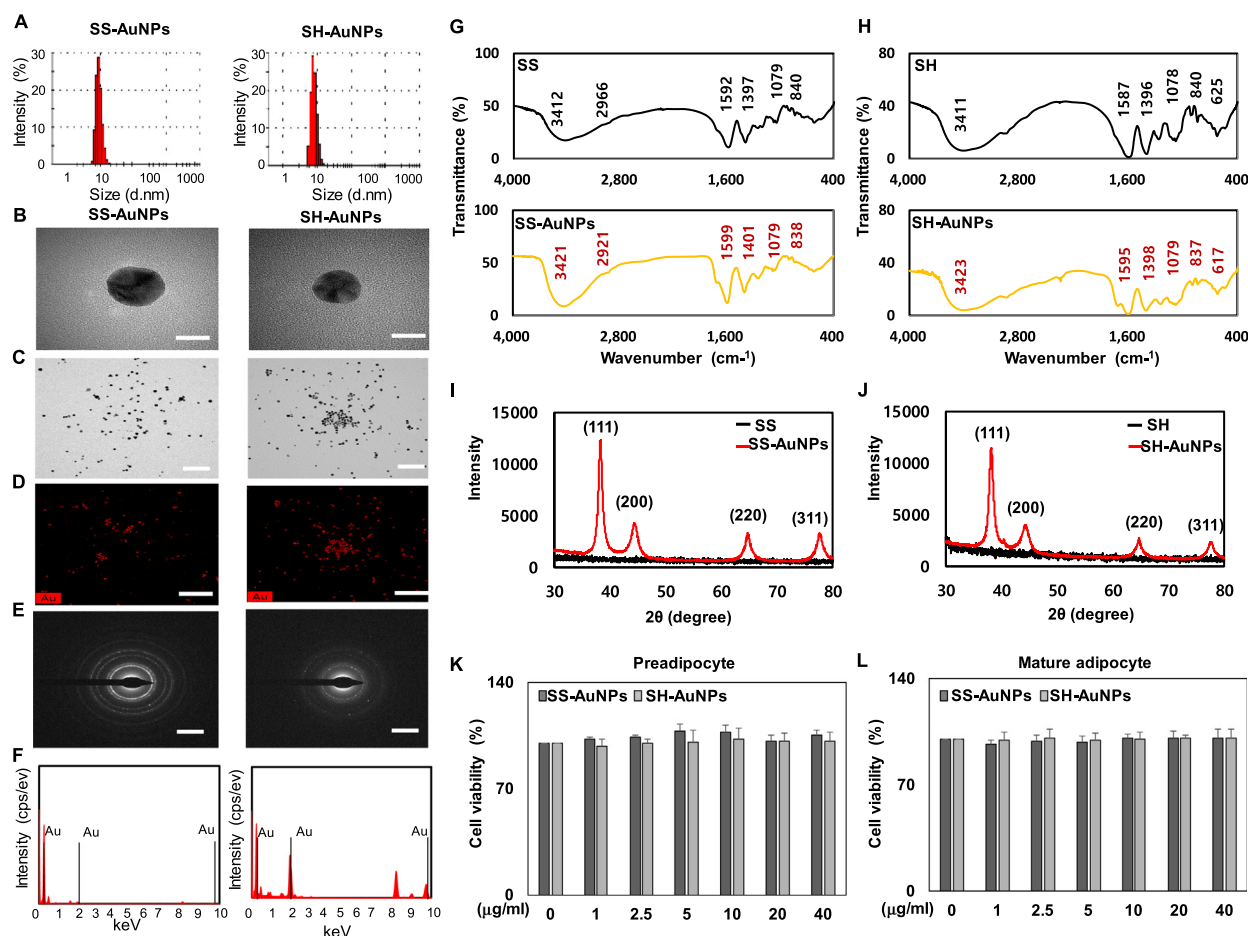


Fig. 2 Physicochemical characterization and cell viability of SS-AuNPs and SH-AuNPs. Hydrodynamic size (A), HR-TEM images at low (B, Scale bar = 10 nm.) and high (C, Scale bar = 200 nm.), HAADF imaging (D, Scale bar = 200 nm.), (E) SAED patterns, (F) EDS, (G, H) FTIR analysis, and (I, J), XRD (K, L) cell viability of SS-AuNPs and SH-AuNPs.

nes, polysaccharides, and others present in SS and SH extracts, act as capping and reducing agents in the synthesis of AuNPs. In addition, the crystalline properties of SS-AuNPs and SH-AuNPs were confirmed by XRD analysis. At $2\theta = 37.77^\circ$, 43.74° , 64.50° and 77.33° , the Bragg reflection peaks correspond to the (111), (200), (220) and (311) planes, respectively. The XRD patterns of SS-AuNPs and SH-AuNPs showed that, unlike SS and SH extracts, these AuNPs had a crystalline structure (Fig. 2I and J).

3.2. Effect of SS-AuNPs and SH-AuNPs on Oil Red-O staining activity and TG accumulation

To investigate the viability of SS-AuNPs and SH-AuNPs against pre- and mature adipocytes, we measured cell viability by using the CCK-8 assay. CCK-8 is an adipocyte viability assay method in which water-soluble tetrazolium salt is reduced to formazan by adipocyte dehydrogenase in a culture medium. Formazan is proportional to the number of living adipocytes and was confirmed through final colorimetric assays. Our results confirmed that there was no effect on cell viability in pre- and mature adipocytes after treatment with SS-AuNPs and SH-AuNPs at concentrations up to 40 μg/mL for 24 h (Fig. 2 K and L). Thus, concentrations of SS-

AuNPs and SH-AuNPs of 10 and 20 μg/mL, respectively, were used in this study. For determining the effect of SS-AuNPs and SH-AuNPs on adipogenic differentiation, lipid accumulation in pre- and mature adipocytes was monitored using an Oil Red-O staining assay. MDI-treated preadipocytes initiated adipogenic differentiation, and Oil Red-O staining indicated marked intracellular lipid droplet accumulation on day 9. Lipid droplet accumulation was not observed in the preadipocytes without MDI induction. The number of globular cells in mature adipocytes was higher in adipocytes treated with MDI for up to 9 d (Fig. 3A). The preadipocytes finally differentiate into mature adipocytes. We cultured pre- and mature adipocytes for 9 d in the presence of SS-AuNPs and SH-AuNPs and then identified lipid droplets that accumulated in the cytoplasm. Adipocytes store lipid droplets related to differentiation into mature adipocytes, and it was confirmed that the accumulation of lipid droplets decreased in adipocytes cultured with SS-AuNPs and SH-AuNPs (Fig. 3A). Quantification of the extracted Oil Red-O staining confirmed that the accumulation of lipid droplets in adipocytes treated with SS-AuNPs and SH-AuNPs (10 and 20 μg/mL, respectively) decreased in a concentration-dependent manner (Fig. 3B). The TG content was measured to investigate the effects of the metabolites on lipid metabolism. Differentiation into mature adipocytes. It

can be confirmed that TGs accumulate as our results showed that MDI-induced TG content in mature adipocytes was significantly increased. SS-AuNPs and SH-AuNPs (10 and 20 $\mu\text{g}/\text{mL}$) reduced intracellular TG levels in a dose-dependent manner, without affecting cell viability. SH-AuNPs inhibited TG accumulation more effectively than SS-AuNPs at the same concentration (Fig. 3C). No significant differences were observed in the Oil Red-O staining activity or TG-accumulation in the pre-adipocyte treatment group. These findings show that SS-AuNPs and SH-AuNPs suppressed lipid accumulation in mature adipocytes.

3.3. Effect of SS-AuNPs and SH-AuNPs on Nile-Red staining activity

Nile-Red Staining Kit (excitation/emission: 550/640 nm) was used for the quantitative fluorescence detection and measurement of intracellular lipid droplets using confocal microscopy and flow cytometry. Nile-red reagent fluoresces only in lipophilic environments and is an excellent reagent for visualizing intracellular lipid droplets through fluorescent staining. Fig. 4A shows a panel of confocal microscopy images for visualizing lipid droplets from pre- and mature adipocytes incubated with Nile-Red solution for 1 h. Mature adipocytes (MDI-induced) showed significantly increased lipid droplets, and pretreatment with SS-AuNPs and SH-AuNPs dramatically reversed the accumulation of lipid droplets (Fig. 4A). Next, we quantified these results: cellular lipid levels in pre-

and mature adipocytes were quantified using flow cytometry (Fig. 4B). Additionally, per the flow cytometry results, cellular lipid levels in mature adipocytes were 67.1% higher than in preadipocytes, and cellular lipid levels in the SS-AuNPs and SH-AuNPs-pretreated groups were reduced to 27.8% and 23.0%, respectively, of those in mature adipocytes (Fig. 4B).

3.4. Effects of SS-AuNPs and SH-AuNPs on the mRNA and protein expression of adipogenesis

Induction of MDI into preadipocytes, whose growth has been stopped by intercellular junctions, initiates differentiation into mature adipocytes. In this process, transcription factors for early adipogenesis, including C/EBP α , SREBP-1, and PPAR, are activated, and these transcription factors interact to promote their expression. This C/EBP α and PPAR interaction induces the expression of FAS and aP2, which are then involved in final lipogenesis (Yan et al., 2022; Qin et al., 2022; Pinto et al., 2021). To detect the effect of SS-AuNPs and SH-AuNPs on the transcription of adipogenic factors, we determined the expression of C/EBP α , PPAR γ , SREBP-1, FAS, and aP2 mRNA in pre- and mature adipocytes. The expression of these genes was significantly higher in mature adipocytes than in preadipocytes. Compared to the mature adipocytes (MDI-induced), the expression of C/EBP α , PPAR γ , SREBP-1, FAS, and aP2 mRNA decreased significantly after pretreatment with SS-AuNPs and SH-AuNPs at a concentration of 20 $\mu\text{g}/\text{mL}$ (Table 4). To further explore

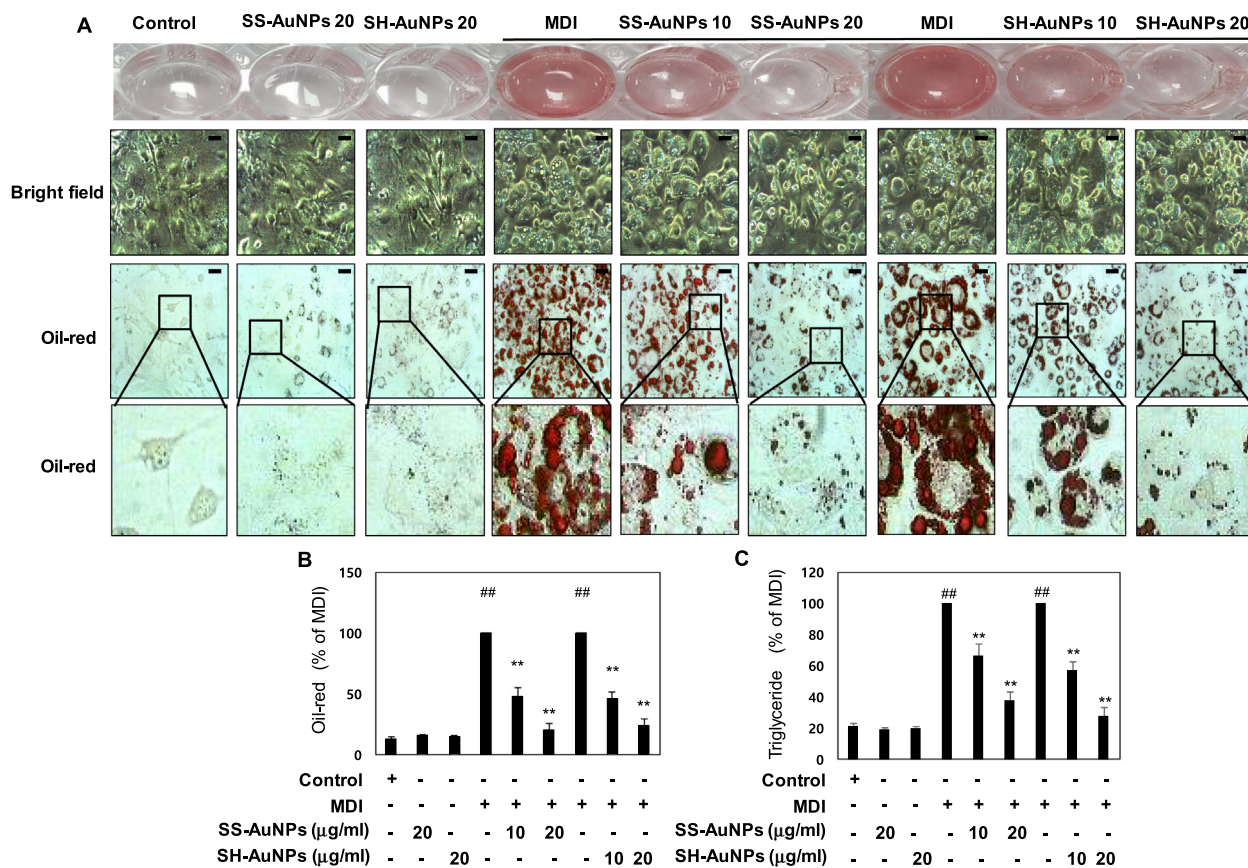


Fig. 3 Oil Red-O staining activity and TG accumulation of SS-AuNPs and SH-AuNPs. (A) Oil Red O staining and morphological changes (B) Quantitation of Oil Red O staining activity (Scale bar = 100 μm) and (C) triglyceride content.

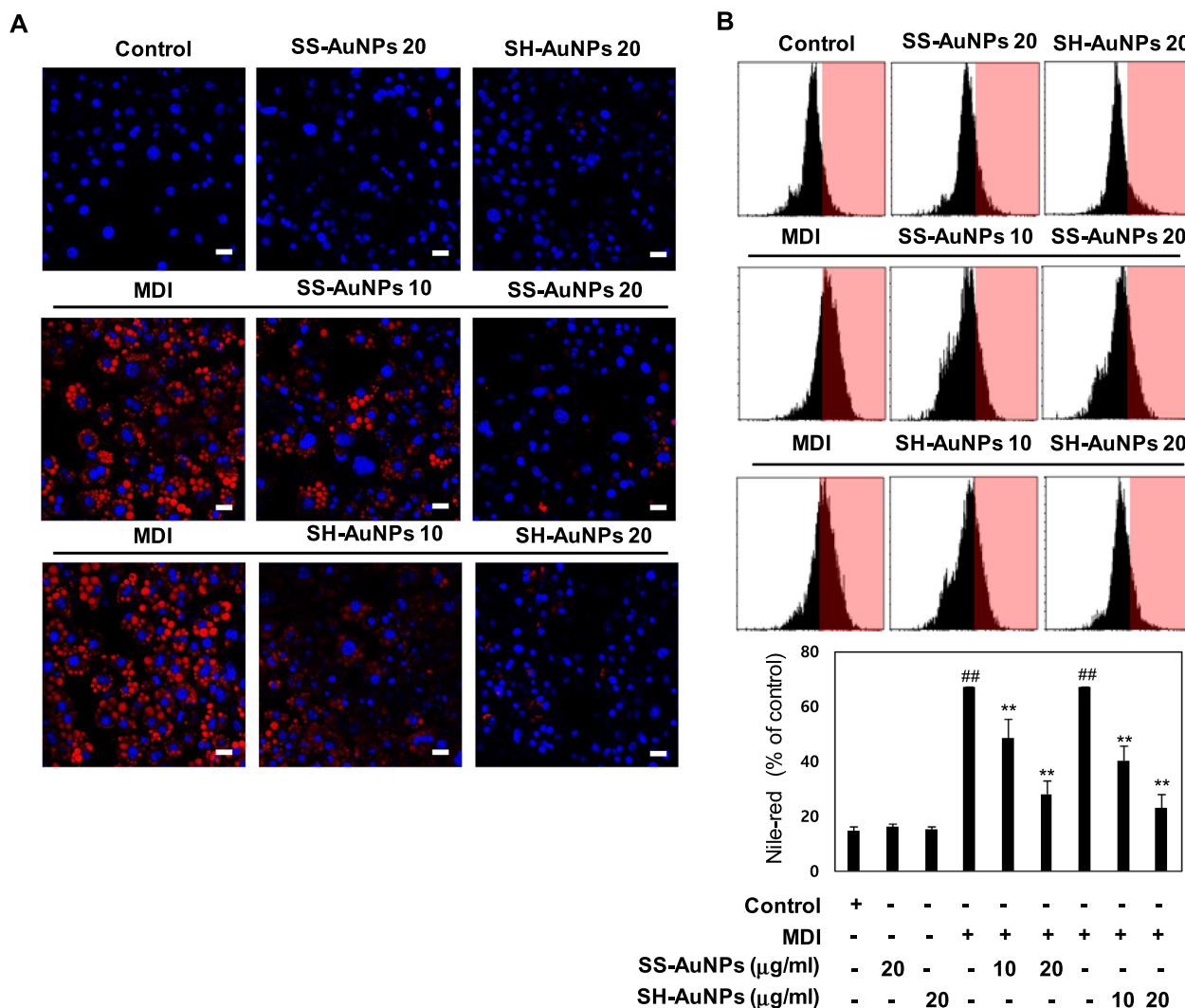


Fig. 4 Nile-Red staining activity of SS-AuNPs and SH-AuNPs. Nile-red staining activity was detected by confocal microscopy (A, Scale bar = 100 μm) Nile-red staining activity was detected by flow cytometry (B).

the effect of SS-AuNPs and SH-AuNPs on the translation of adipogenic factors in mature adipocytes, we determined the expression of C/EBP α , PPAR γ , SREBP-1, FAS, and aP2 proteins in pre- and mature adipocytes. Compared to preadipocytes, mature adipocytes (MDI-induced) showed significant upregulation of the expression of C/EBP α , PPAR γ , SREBP-1, FAS, and aP2, and these effects were downregulated by the pretreatment with SS-AuNPs and SH-AuNPs (Fig. 5). In addition, the mRNA and protein expression of C/EBP α , PPAR γ , SREBP-1, FAS, and aP2 in pre-adipocytes were not significantly different from those in the control group when pretreated with 20 $\mu\text{g/ml}$ SS-AuNPs and SH-AuNPs. These results demonstrated that SS-AuNPs and SH-AuNPs exhibited anti-adipogenic activity by downregulating adipogenic factors.

3.5. Effects of SS-AuNPs and SH-AuNPs on the mitochondrial thermogenesis in mature adipocyte

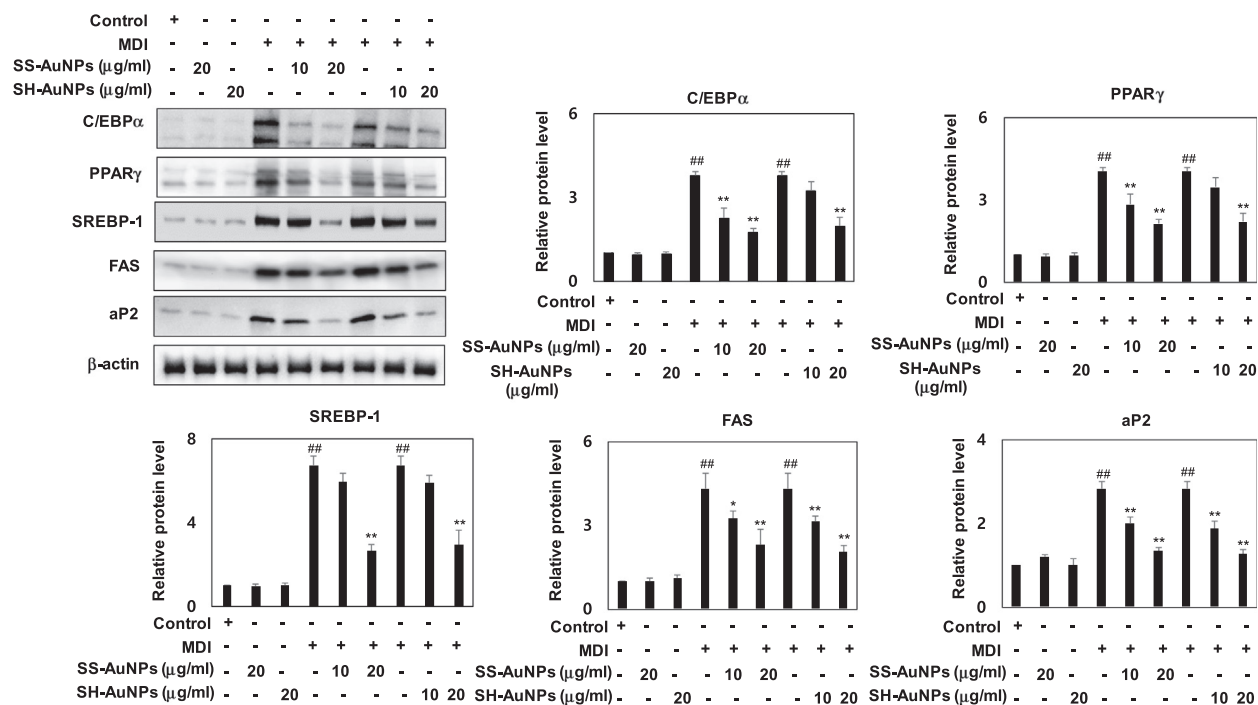
White adipocytes and brown adipocytes are present in adipose tissue. White adipocytes store excess energy, such as TGs, whereas brown adipocytes simultaneously have high UCP1

expression and a large number of mitochondria. These brown adipocytes contribute to the regulation of energy expenditure stored in adipocytes (Zhao, B. et al., 2021; Zhao, D. et al., 2021; Gu et al., 2021). Immunofluorescence was performed to confirm mitochondrial biogenesis and UCP1 expression and characteristics of brown adipocytes. Mature adipocytes were stained with MitoTracker (red), which specifically binds to mitochondria, and then with FITC (green)-conjugated UCP1 antibody. In the case of SS-AuNPs and SH-AuNPs pretreatment, more intense red fluorescence was observed in the cytoplasm of mature adipocytes, and UCP1 also exhibited mitochondrial colocalization in the cytoplasm (Fig. 6A). PGC-1 α , an important regulator of mitochondrial biogenesis and characteristic of brown adipocytes, induces the expression of UCP1 and PRDM16, and PRDM16 acts as an important factor in the development of brown adipocytes (Botezelli et al., 2020; Park, S. J. et al., 2019). To further investigate the mechanism of the browning effect of SS-AuNPs and SH-AuNPs, we measured the mRNA and protein expression levels of phosphorylated UCP1, PRDM16, and PGC1 α . In mature adipocytes, the SS-AuNPs and SH-AuNPs pretreatments sig-

Table 4 mRNA expression of *C/EBP α* , *PPAR γ* , *SREBP-1*, *FAS* and *Adiponectin* gene of each group.

	<i>C/EBPα</i>	<i>PPARγ</i>	<i>SREBP-1</i>	<i>FAS</i>	<i>Ap2</i>
control	0.08 ± 0.02	0.04 ± 0.01	0.08 ± 0.02	0.09 ± 0.02	0.07 ± 0.03
SS-GNP (20 μ g/ml)	0.07 ± 0.01	0.05 ± 0.02	0.07 ± 0.01	0.06 ± 0.02	0.08 ± 0.02
SH-GNP (20 μ g/ml)	0.08 ± 0.02	0.05 ± 0.01	0.08 ± 0.02	0.06 ± 0.02	0.07 ± 0.02
MDI	1.00 ± 0.03 ^{##}	1.00 ± 0.04 ^{##}	1.00 ± 0.03 ^{##}	1.00 ± 0.03 ^{##}	1.00 ± 0.03 ^{##}
SS-GNP (10 μ g/ml) + MDI	0.64 ± 0.04 ^{**}	0.75 ± 0.05 [*]	0.64 ± 0.04 ^{**}	0.65 ± 0.04 ^{**}	0.76 ± 0.06 [*]
SS-GNP (20 μ g/ml) + MDI	0.32 ± 0.04 ^{**}	0.23 ± 0.05 ^{**}	0.32 ± 0.04 ^{**}	0.26 ± 0.05 ^{**}	0.15 ± 0.03 ^{**}
SH-GNP (10 μ g/ml) + MDI	0.70 ± 0.04 [*]	0.70 ± 0.01 [*]	0.70 ± 0.04 [*]	0.79 ± 0.03 [*]	0.69 ± 0.05 [*]
SH-GNP (20 μ g/ml) + MDI	0.19 ± 0.06 ^{**}	0.25 ± 0.05 ^{**}	0.19 ± 0.06 ^{**}	0.20 ± 0.03 ^{**}	0.20 ± 0.08 ^{**}

Note: *P < 0.05, **P < 0.01.

**Fig. 5** Downregulation of *C/EBP α* , *PPAR γ* , *SREBP-1*, *FAS*, and *aP2* by SS-AuNPs and SH-AuNPs. (A) Effect of SS-AuNPs and SH-AuNPs on *C/EBP*, *PPAR*, *SREBP-1*, *FAS*, and *aP2* expression.

nificantly upregulated the mRNA expression of *UCP1*, *PRDM16*, and *PGC1 α* (Table 5). The protein levels of *UCP1*, *PRDM16*, and *PGC1 α* were also evaluated. The pretreatment of mature adipocytes with SS-AuNPs and SH-AuNPs increased the protein expression of *UCP1*, *PRDM16*, and *PGC1 α* . These results suggest that SS-AuNPs and SH-AuNPs can upregulate mitochondrial biogenesis in mature adipocytes and increase the expression of brown adipogenesis marker genes.

4. Discussion

AuNPs are classified as nanomaterials that constitute an ideal platform for various biomedical applications by constituting all types of structured nanoparticles through a single physicochemical property (Holišová et al., 2021; Lee, K. X. et al., 2020). The exponential increase in the production of AuNPs places a substantial burden on the environment. In the past

decade, research has been conducted to devise new eco-friendly and inexpensive synthesis methods that deviate from the existing approaches that toxic chemicals. Plant extracts, plant biomolecules, and biological materials such as bacteria, fungi, and algae are eco-friendly approaches for safe, alternate modes of production (Nayem et al., 2020; Lee, K. X. et al., 2020; Khan et al., 2019). SS and SH are traditional Chinese medicines that are abundant in the coastal waters of China, Japan, and Korea. SS and SH are edible brown algae used as savory, nutritious sea vegetables in China and Korea. Additionally, studies on the treatment and prevention of metabolic syndromes, such as diabetes, obesity, high blood pressure, and hyperlipidemia using SS and SH have been conducted (Kim et al., 2021; Fernando et al., 2021; Herath et al., 2021). The major biomolecules of SS and SH include sterols such as sulfated polysaccharides, fucosterol, and cholesterol, and various functional groups such as muramic acid, glucuronic acid, alginate, and vinyl derivatives, which can act as reducing and

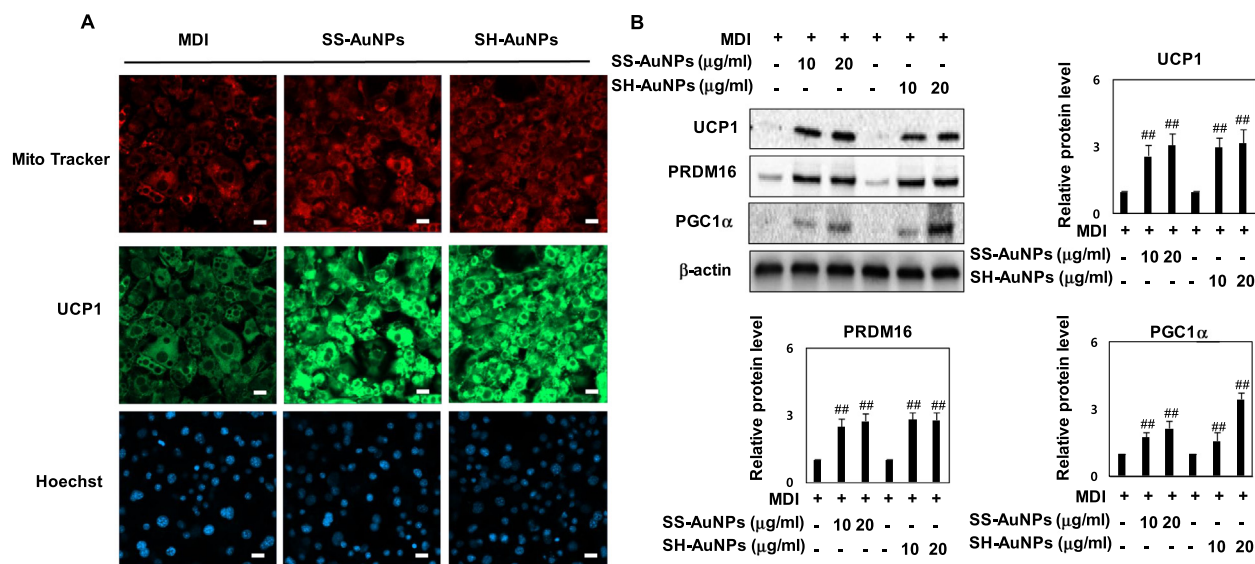


Fig. 6 Upregulation of mitochondrial thermogenesis by SS-AuNPs and SH-AuNPs. (A) Effect of SS-AuNPs and SH-AuNPs on mitochondrial biogenesis. Scale bar = 100 μ m. (B) Effect of SS-AuNPs and SH-AuNPs on UCP1, PRDM16, and PGC1 α expression.

Table 5 mRNA expression of *UCP1*, *PRDM16* and *PGC1 α* of each group.

	<i>UCP1</i>	<i>PRDM16</i>	<i>PGC1α</i>
MDI	1.00 \pm 0.01	1.00 \pm 0.03	1.00 \pm 0.01
SS-GNP (10 mg/ml) + MDI	3.12 \pm 0.23*	2.81 \pm 0.17	3.06 \pm 0.48*
SS-GNP (20 mg/ml) + MDI	7.30 \pm 0.29**	5.70 \pm 0.72**	8.12 \pm 0.78**
SH-GNP (10 mg/ml) + MDI	2.62 \pm 0.42	3.43 \pm 0.31*	3.70 \pm 0.34*
SH-GNP (20 mg/ml) + MDI	7.97 \pm 0.92**	7.26 \pm 0.91**	8.39 \pm 0.41**

Note: *P < 0.05, **P < 0.01.

capping agents and surface-bound proteins; these residual amino acids in nanoparticles help cap and stabilize nanoparticles (Ko et al., 2021; Han, Kim et al., 2021; Han, Jayawardena et al., 2021). Therefore, in this study, extracts of SS and SH, representing brown algae, were used as reducing-capping and stabilizing agents for AuNPs synthesis. SH and SS extracts covering the surface are eco-friendly, biocompatible, and serve as functional residues compared with the base chemical. The formation of SS-AuNPs and SH-AuNPs was confirmed by observing the color change from pale yellow to red-violet in the SS and SH extracts with maximum SPR peaks at 528 nm and 525 nm, respectively. The crystal structure and spherical shape (size: 17.4–21.0 nm) were confirmed by DLS and HR-TEM analysis, respectively. Based on the FTIR results, the functional groups present in the SS and SH extracts were analyzed to determine their role in the reduction, capsulation, and stabilization processes. Notably, there are limitations to analyzing the exact mechanism and active ingredients involved in the biosynthesis of SS-AuNPs and SH-AuNPs. Several environmental conditions (eg pH, pressure, temperature) are considered to influence rather than simply biosynthesis by the biological components of an applied organism. An easily used method for the synthesis of AuNPs is the reduction of chemicals by a reducing agent in the presence of a stabilizer. Unfortunately, many reducing agents consume capital and energy, and many toxic chemicals such as surfactants and thiols are used. However, synthesis from algae affords AuNPs that are

cost-effective, clean and harmless to the environment. Nevertheless, recent studies have not yet fully demonstrated the complex interactions between AuNPs synthesized by algae.

Obesity is a global health problem in modern society, and many studies are being conducted to alleviate obesity-related complications. Obesity is related to the enlargement of adipose tissue by the accumulation of TGs and the production of lipids, which is an energy source for adipocytes (Yang et al., 2021; Soundharrajan et al., 2020; Moon et al., 2013). Obesity results from an energy imbalance that can be controlled through lipid metabolism in adipocytes. Many studies have been conducted to suppress adipogenesis by reducing the differentiation into mature adipocytes using preadipocytes (Lim et al., 2021; Du et al., 2022; Qin et al., 2022). This study investigated the anti-adipogenic effects of SS-AuNPs and SH-AuNPs through a reliable adipogenesis-related mechanism. Adipose tissue enlargement is proportional to the size and number of lipid droplets in mature adipocytes. We confirmed that SS-AuNPs and SH-AuNPs reduced lipid droplets in mature adipocytes by using Oil Red-O and Nile-Red staining methods. TGs are a major form of fatty acid storage in adipocytes and other tissues whose increased intracellular accumulation may contribute to obesity. TG production was inhibited by SS-AuNPs and SH-AuNPs. Further studies were conducted to elucidate the signaling mechanisms related to lipid metabolism in adipocytes by reducing lipid accumulation in the SS-AuNPs and SH-AuNPs groups. PPAR- γ and C/EBP α ,

SREBP-1c act as major adipogenic transcription factors in adipocyte differentiation and lipid droplet formation. These genes regulate the transcription of FAS, a multienzyme protein catalyzing fatty acid synthesis in adipocytes, and aP2, which promotes transport of lipids to specific cellular compartments through storage of lipid droplets. In particular, SREBP-1c increases the expression of genes involved in fatty acid biosynthesis and triglyceride maturation, and PPAR- γ promotes glucose metabolism, leading to C/EBP α expression and activation. Together with PPAR- γ and C/EBP α , SREBP-1c is a central regulatory transcription factor for preadipocyte differentiation, and these genes are linked to FAS and aP2 as adipose-specific enhancers. Specifically, FAS and aP2 are markers of mature adipocytes responsible for morphological changes in adipocytes and lipid accumulation. We confirmed that SS-AuNPs and SH-AuNPs repressed the transcription and translation of PPAR γ , C/EBP α , SREBP-1c, FAS, and aP2 genes. These results suggest that SS-AuNPs and SH-AuNPs exert an anti-adipogenic effect by reducing these transcription factors and mature adipocyte markers in adipocytes.

In mammalian adipose tissue, white adipocytes store energy, and brown adipocytes consume energy. Brown adipocytes have abundant mitochondria and convert energy into heat via rapid glucose consumption and fatty acid oxidation by separating the respiratory chain (Rahman and Kim, 2020; Bai et al., 2021; Hao et al., 2020). Controlling obesity through energy consumption by promoting brown fat in white adipocytes is being investigated as a potential therapeutic strategy. UCP1, PRDM16, and PGC1 α are representative markers for inducing brown adipogenesis in adipocytes with the ability to generate heat. UCP1 is a mitochondrial inner membrane protein that plays an important role in dissipating energy from adipocytes in relation to mitochondrial biogenesis and thermogenesis. PGC-1 α , a transcriptional coactivator of UCP1, can stimulate peroxisomal activity, the expression of the tricarboxylic acid cycle, and mitochondrial fatty acid oxidation. PRDM16 also plays an important role in increasing mitochondrial function and gene expression and promoting brown adipogenesis in adipocytes (Tang et al., 2021; Park, S. J. et al., 2019; Botezelli et al., 2020). In this study, SS-AuNPs and SH-AuNPs effectively induced brown adipogenesis in mature adipocytes, leading to small multilocular lipid droplets and increased mitochondrial biogenesis. In contrast, it was confirmed that the transcription and translation of UCP1, PRDM16, and PGC1 α , which are representative markers of brown adipogenesis in adipocytes, were also upregulated by SS-AuNPs and SH-AuNPs.

5. Conclusion

The facile, eco-friendly, and non-hazardous synthesis of SS-AuNPs and SH-AuNPs has been successfully prepared using extracts of SS and SH as reducing agents, capping agents, and stabilizing agents. The formation of SS-AuNPs and SH-AuNPs was confirmed by UV-spec, DLS, HR-TEM, EDS analyses. Based on cell-based experiments, we demonstrated that SS-AuNPs and SH-AuNPs can reduce lipid accumulation in adipocytes by downregulating adipogenesis target proteins and upregulating brown adipogenesis. We also found that the pretreatment with SS-AuNPs and SH-AuNPs in mature adipocytes downregulated the protein expression of PPAR γ , C/EBP α , SREBP-1c, FAS, and aP2 genes and upregulated UCP1, PRDM16, and

PGC1 α expression and mitochondrial biogenesis. These results demonstrate the potential pharmacological effects of SS-AuNPs and SH-AuNPs in obesity-related metabolic syndrome.

Declaration of Competing Interest

The authors declare that they have no known competing financial interests or personal relationships that could have appeared to influence the work reported in this paper.

Acknowledgements

This research was supported by the Basic Science Research Program of the National Research Foundation of Korea (NRF), which was funded by the Ministry of Education, Science, and Technology (NRF-2021R1I1A3A04035369).

Disclosure

The authors declare that the research was conducted in the absence of any commercial or financial relationships that could be construed as potential conflicts of interest.

References

- Abbas, M.A., Boby, N., Lee, E.B., Hong, J.H., Park, S.C., 2022. Anti-obesity effects of ecklonia cava extract in high-fat diet-induced obese rats. *Antioxidants (Basel)* 11, 310. <https://doi.org/10.3390/antiox11020310>.
- Andleeb, A., Andleeb, A., Asghar, S., Zaman, G., Tariq, M., Mehmood, A., Nadeem, M., Hano, C., Lorenzo, J.M., Abbasi, B.H., 2021. A systematic review of biosynthesized metallic nanoparticles as a promising anti-cancer-strategy. *Cancers (Basel)* 13, 2818. <https://doi.org/10.3390/cancers13112818>.
- Bai, N., Ma, J., Alimujiang, M., Xu, J., Hu, F., Xu, Y., Leng, Q., Chen, S., Li, X., Han, J., Jia, W., Bao, Y., Yang, Y., 2021. Bola3 regulates beige adipocyte thermogenesis via maintaining mitochondrial homeostasis and lipolysis. *Front. Endocrinol. (Lausanne)* 11, 592154.
- Boomi, P., Ganesan, R., Prabu Poorani, G., Jegatheeswaran, S., Balakumar, C., Gurumalles Prabu, H., Anand, K., Marimuthu Prabhu, N., Jeyakanthan, J., Saravanan, M., 2020. Phyto-engineered gold nanoparticles (AuNPs) with potential antibacterial, antioxidant, and wound healing activities under in vitro and in vivo conditions. *Int. J. Nanomed.* 15, 7553–7568.
- Borah, A.K., Sharma, P., Singh, A., Kalita, K.J., Saha, S., Chandra Borah, J., 2021. Adipose and non-adipose perspectives of plant derived natural compounds for mitigation of obesity. *J. Ethnopharmacol.* 280, 114410.
- Botezelli, J.D., Overby, P., Lindo, L., Wang, S., Haïda, O., Lim, G.E., Templeman, N.M., Pauli, J.R., Johnson, J.D., 2020. Adipose depot-specific upregulation of Ucp1 or mitochondrial oxidative complex proteins are early consequences of genetic insulin reduction in mice. *Am. J. Physiol. Endocrinol. Metab.* 319, E529–E539.
- Dias, M.K.H.M., Madusanka, D.M.D., Han, E.J., Kim, H.S., Jeon, Y.J., Jee, Y., Kim, K.N., Lee, K., Fernando, I.P.S., Ahn, G., 2021. *Sargassum horneri* (Turner) C. Agardh ethanol extract attenuates fine dust-induced inflammatory responses and impaired skin barrier functions in HaCaT keratinocytes. *J. Ethnopharmacol.* 273, 114003.
- Du, Y., Li, D.X., Lu, D.Y., Zhang, R., Zhong, Q.Q., Zhao, Y.L., Zheng, X.X., Ji, S., Wang, L., Tang, D.Q., 2022. Amelioration of lipid accumulations and metabolism disorders in differentiation

- and development of 3T3-L1 adipocytes through mulberry leaf water extract. *Phytomedicine* 98, 153959.
- Fernando, I.P.S., Dias, M.K.H.M., Madusanka, D.M.D., Han, E.J., Kim, M.J., Jeon, Y.J., Ahn, G., 2020. Step gradient alcohol precipitation for the purification of low molecular weight fucoidan from *Sargassum siliquastrum* and its UVB protective effects. *Int. J. Biol. Macromol.* 163, 26–35.
- Fernando, I.P.S., Heo, S.J., Dias, M.K.H.M., Madusanka, D.M.D., Han, E.J., Kim, M.J., Sanjeeva, K.K.A., Lee, K., Ahn, G., 2021. (-)-Loliolide isolated from *Sargassum horneri* Abate UVB-induced oxidative damage in human dermal fibroblasts and subside ECM degradation. *Mar. Drugs* 19, 435. <https://doi.org/10.3390/md19080435>.
- Gu, Y., Xiao, X., Pan, R., Zhang, J., Zhao, Y., Dong, Y., Cui, H., 2021. *Lactobacillus plantarum* dy-1 fermented barley extraction activates white adipocyte browning in high-fat diet-induced obese rats. *J. Food Biochem.* 45, e13680.
- Han, E.J., Jayawardena, T.U., Jang, J.H., Fernando, I.P.S., Jee, Y., Jeon, Y.J., Lee, D.S., Lee, J.M., Yim, M.J., Wang, L., Kim, H.S., Ahn, G., 2021. Sargachromenol purified from *sargassum horneri* inhibits inflammatory responses via activation of Nrf2/HO-1 signaling in LPS-stimulated macrophages. *Mar. Drugs* 19, 497. <https://doi.org/10.3390/md19090497>.
- Hao, M., Guan, Z., Gao, Y., Xing, J., Zhou, X., Wang, C., Xu, J., Li, W., 2020. Huang-Qi San ameliorates hyperlipidemia with obesity rats via activating brown adipocytes and converting white adipocytes into brown-like adipocytes. *Phytomedicine* 78, 153292.
- Herath, K.H.I.N.M., Cho, J., Kim, H.J., Dinh, D.T.T., Kim, H.S., Ahn, G., Jeon, Y.J., Jee, Y., 2021. Polyphenol containing *Sargassum horneri* attenuated Th2 differentiation in splenocytes of ovalbumin-sensitized mice: involvement of the transcription factors GATA3/STAT5/NLRP3 in Th2 polarization. *Pharm. Biol.* 59, 1464–1472.
- Ho, J.N., Son, M.E., Lim, W.C., Lim, S.T., Cho, H.Y., 2012. Anti-obesity effects of germinated brown rice extract through down-regulation of lipogenic genes in high fat diet-induced obese mice. *Biosci. Biotechnol. Biochem.* 76, 1068–1074.
- Holišová, V., Urban, M., Konvičková, Z., Kolenčík, M., Mančík, P., Slabotinský, J., Kratošová, G., Plachá, D., 2021. Colloidal stability of phytosynthesised gold nanoparticles and their catalytic effects for nerve agent degradation. *Sci. Rep.* 11, 4071-021-83460-1.
- Jee, W., Lee, S.H., Ko, H.M., Jung, J.H., Chung, W.S., Jang, H.J., 2021. Anti-obesity effect of polygalin C isolated from *Polygala japonica* Houtt. via suppression of the adipogenic and lipogenic factors in 3T3-L1 adipocytes. *Int. J. Mol. Sci.* 22, 10405. <https://doi.org/10.3390/ijms221910405>.
- Jun, E.S., Kim, Y.J., Kim, H.H., Park, S.Y., 2020. Gold nanoparticles using *Ecklonia stolonifera* protect human dermal fibroblasts from UVA-induced senescence through inhibiting MMP-1 and MMP-3. *Mar. Drugs* 18, 433. <https://doi.org/10.3390/md18090433>.
- Khan, T., Ullah, N., Khan, M.A., Mashwani, Z.U., Nadhman, A., 2019. Plant-based gold nanoparticles; a comprehensive review of the decade-long research on synthesis, mechanistic aspects and diverse applications. *Adv. Colloid Interface Sci.* 272, 102017.
- Kim, E.N., Nabende, W.Y., Jeong, H., Hahn, D., Jeong, G.S., 2021. The marine-derived natural product epiloliolide isolated from *Sargassum horneri* regulates NLRP3 via PKA/CREB, promoting proliferation and anti-inflammatory effects of human periodontal ligament cells. *Mar. Drugs* 19, 388. <https://doi.org/10.3390/md19070388>.
- Ko, W., Lee, H., Kim, N., Jo, H.G., Woo, E.R., Lee, K., Han, Y.S., Park, S.R., Ahn, G., Cheong, S.H., Lee, D.S., 2021. The antioxidative and anti-neuroinflammatory effects of *Sargassum horneri* by Heme Oxygenase-1 induction in BV2 and HT22 cells. *Antioxidants (Basel)* 10, 859. <https://doi.org/10.3390/antiox10060859>.
- Lee, J.I., Kwak, M.K., Park, H.Y., Seo, Y., 2013. Cytotoxicity of meroterpenoids from *Sargassum siliquastrum* against human cancer cells. *Nat. Prod. Commun.* 8, 431–432.
- Lee, K.X., Shamel, K., Yew, Y.P., Teow, S.Y., Jahangirian, H., Rafiee-Moghaddam, R., Webster, T.J., 2020. Recent developments in the facile bio-synthesis of gold nanoparticles (AuNPs) and their biomedical applications. *Int. J. Nanomed.* 15, 275–300.
- Lim, S.H., Lee, H.S., Han, H.K., Choi, C.I., 2021. Saikosaponin A and D inhibit adipogenesis via the AMPK and MAPK signaling pathways in 3T3-L1 adipocytes. *Int. J. Mol. Sci.* 22, 11409. <https://doi.org/10.3390/ijms222111409>.
- Machado, S., González-Ballesteros, N., Gonçalves, A., Magalhães, L., Pereira, S., de Passos, M., Rodríguez-Argüelles, M.C., Castro Gomes, A., 2021. Toxicity in vitro and in Zebrafish embryonic development of gold nanoparticles biosynthesized using *cystoseira* macroalgae extracts. *Int. J. Nanomed.* 16, 5017–5036.
- Molina-Ayala, M.A., Rodríguez-Amador, V., Suárez-Sánchez, R., León-Solis, L., Gómez-Zamudio, J., Mendoza-Zubieta, V., Cruz, M., Suárez-Sánchez, F., 2022. Expression of obesity- and type-2 diabetes-associated genes in omental adipose tissue of individuals with obesity. *Gene* 815, 146181.
- Moon, J., Do, H.J., Kim, O.Y., Shin, M.J., 2013. Antiobesity effects of quercetin-rich onion peel extract on the differentiation of 3T3-L1 preadipocytes and the adipogenesis in high fat-fed rats. *Food Chem. Toxicol.* 58, 347–354.
- Nayem, S.M.A., Sultana, N., Haque, M.A., Miah, B., Hasan, M.M., Islam, T., Hasan, M.M., Awal, A., Uddin, J., Aziz, M.A., Ahammad, A.J.S., 2020. Green synthesis of gold and silver nanoparticles by using *amorphophallus paeoniifolius* tuber extract and evaluation of their antibacterial activity. *Molecules* 25, 4773. <https://doi.org/10.3390/molecules25204773>.
- Park, M., Baek, H., Han, J.Y., Lee, H.J., 2022. Stevioside enhances the anti-adipogenic effect and β -oxidation by activating AMPK in 3T3-L1 cells and epididymal adipose tissues of db/db mice. *Cells* 11, 1076. <https://doi.org/10.3390/cells11071076>.
- Park, S.J., Park, M., Sharma, A., Kim, K., Lee, H.J., 2019. Black ginseng and ginsenoside Rb1 promote browning by inducing UCPI expression in 3T3-L1 and primary white adipocytes. *Nutrients* 11, 2747. <https://doi.org/10.3390/nu1112747>.
- Park, S.Y., Kim, B., Cui, Z., Park, G., Choi, Y.W., 2020. Anti-Metastatic effect of gold nanoparticle-conjugated *Maclura tricuspidata* extract on human hepatocellular carcinoma cells. *Int. J. Nanomed.* 15, 5317–5331.
- Pinto, C., Ibáñez, M.R., Loyola, G., León, L., Salvatore, Y., González, C., Barraza, V., Castañeda, F., Aldunate, R., Contreras-Porcía, L., Fuenzalida, K., Bronfman, F.C., 2021. Characterization of an Agarophyton chilense oleoresin containing PPAR γ natural ligands with insulin-sensitizing effects in a C57Bl/6J mouse model of diet-induced obesity and antioxidant activity in *caenorhabditis elegans*. *Nutrients* 13, 1828. <https://doi.org/10.3390/nu13061828>.
- Qin, H., Song, Z., Zhao, C., Yang, J., Xia, F., Wang, L., Ali, A., Zheng, W., 2022. Liquiritigenin inhibits lipid accumulation in 3T3-L1 cells via mTOR-mediated regulation of the autophagy mechanism. *Nutrients* 14, 1287. <https://doi.org/10.3390/nu14061287>.
- Rahman, M.S., Kim, Y.S., 2020. Mangiferin induces the expression of a thermogenic signature via AMPK signaling during brown-adipocyte differentiation. *Food Chem. Toxicol.* 141, 111415.
- Ree, J., Kim, J.I., Lee, C.W., Lee, J., Kim, H.J., Kim, S.C., Sohng, J. K., Park, Y.I., 2021. Quinizarin suppresses the differentiation of adipocytes and lipogenesis in vitro and in vivo via downregulation of C/EBP-beta/SREBP pathway. *Life Sci.* 287, 120131.
- Soundharajan, I., Kuppusamy, P., Srisesharam, S., Lee, J.C., Sivanesan, R., Kim, D., Choi, K.C., 2020. Positive metabolic effects of selected probiotic bacteria on diet-induced obesity in mice are associated with improvement of dysbiotic gut microbiota. *FASEB J.* 34, 12289–12307.
- Sprengr, S., Woldemariam, T., Kotchoni, S., Elshabrawy, H.A., Chaturvedi, L.S., 2022. Lemongrass essential oil and its major constituent citral isomers modulate adipogenic gene expression in 3T3-L1 cells. *J. Food Biochem.* 46, e14037.

- Tang, Q., Lu, M., Xu, B., Wang, Y., Lu, S., Yu, Z., Jing, X., Yuan, J., 2021. Electroacupuncture regulates inguinal white adipose tissue browning by promoting Sirtuin-1-dependent PPAR γ deacetylation and mitochondrial biogenesis. *Front. Endocrinol. (Lausanne)* 11, 607113.
- Vasileva, L.V., Savova, M.S., Tews, D., Wabitsch, M., Georgiev, M.I., 2021. Rosmarinic acid attenuates obesity and obesity-related inflammation in human adipocytes. *Food Chem. Toxicol.* 149, 112002.
- Yan, H., Li, Q., Li, M., Zou, X., Bai, N., Yu, Z., Zhang, J., Zhang, D., Zhang, Q., Wang, J., Jia, H., Wu, Y., Hou, Z., 2022. Ajuba functions as a co-activator of C/EBP β to induce expression of PPAR γ and C/EBP α during adipogenesis. *Mol. Cell. Endocrinol.* 539, 111485.
- Yang, Y., Zhang, Y., Zhou, X., Chen, D., Ouyang, G., Liu, Y., Cui, D., 2021. Periostin deficiency attenuates lipopolysaccharide- and obesity-induced adipose tissue fibrosis. *FEBS Lett.* 595, 2099–2112.
- Zhao, B., Liu, M., Liu, H., Xie, J., Yan, J., Hou, X., Liu, J., 2021. Zeaxanthin promotes browning by enhancing mitochondrial biogenesis through the PKA pathway in 3T3-L1 adipocytes. *Food Funct.* 12, 6283–6293.
- Zhao, D., Pan, Y., Yu, N., Bai, Y., Ma, R., Mo, F., Zuo, J., Chen, B., Jia, Q., Zhang, D., Liu, J., Jiang, G., Gao, S., 2021. Curcumin improves adipocytes browning and mitochondrial function in 3T3-L1 cells and obese rodent model. *R. Soc. Open Sci.* 8, 200974.